BULK ELASTIC CONSTANTS AND THEIR ROLE IN DIFFRACTIVE STRESS ANALYSIS

Thomas Gnaupel-Herold
NIST Center for Neutron Research
100 Bureau Dr. M/S 6102
Email: tg-h@nist.gov

ABSTRACT

The accuracy of stress determination depends to a large extent on the accuracy to which the diffraction elastic constants (DEC) are available. Calculations of DEC require primarily single crystal elastic constants as input; however, large disparities between elastic properties of multiphase composites generally lead to commensurate differences between the elastic response of individual phases and the response of the aggregate. As a result, the diffractive elastic response of a constituent phase can be quite different compared to that of the single phase polycrystal, thus presenting the need for either measuring or calculating the macroscopic elastic constants as a necessary ingredient for calculating DEC of the respective phase. This work examines a porous material where voids take on the role of a second phase. The theoretical framework for calculating both bulk elastic constants and DEC of a porous aggregate is presented with particular focus on void orientation, aspect ratio and overall porosity. The comparison with published experimental results measured on air plasma sprayed coatings demonstrates good agreement with theoretical estimates if some assumptions are made about void orientation and void aspect ratio. Bulk elastic constants decrease strongly with increasing porosity and, through the grain-matrix interaction effect, the diffraction elastic constants decrease as well, albeit more moderately.

INTRODUCTION

DEC describe the elastic behavior of grains with a common orientation direction. Therefore, models for DEC calculation are specialized cases of calculations of bulk elastic constants. The earliest developed models assumed either that all grains have the same strain (Voigt, 1928) or that all grains have the same stress (Reuss, 1929); both models are upper and lower bound estimates that often yield large differences between estimated and observed elastic constants. There are no mechanisms for considering effects of grain-matrix interaction which also applies for the more useful Hill average (Hill, 1952) of Voigt and Reuss. These models, although simple to use, and, in the case of the Hill average with good agreement to measured bulk constants, have in common that each phase in a multi-phase aggregate is treated independently regardless of phase fraction or the properties of other constituents, thus resulting in often large differences between observed and calculated DEC values (Hauk, 1999).

Considerable progress was made first when Eshelby (Eshelby, 1957) calculated the elastic polarization of an ellipsoidal grain in a homogeneous matrix, thus providing a mechanism for

Bulk Elastic Constants and their Role in Diffractive Stress Analysis" Gnaeupel-Herold, T., Advances in X-ray Analysis 67, (2024)
See here: https://www.icdd.com/axa-allvolumes/#vol67

calculating grain shape dependent elastic grain-matrix interaction. Kröner (1958) subsequently used the Eshelby result, and he developed the self-consistent upper and lower bounds for bulk elastic constants. The Kröner bounds are much tighter then the Reuss/Voigt bounds; they coincide for spherical grains regardless of texture (Kneer, 1965). The DEC models based on the Kröner bounds (Behnken & Hauck, 1986; Gnäupel-Herold *et al.*, 2012) produce different results regardless of grain shape or texture. Experimental evidence suggests a complex picture where in some circumstances (texture, elongated grain shapes, directions of the scattering vector between the surface normal and the in-plane directions) the inverse Kröner model (Gnäupel-Herold *et al.*, 2012, 2011, 2014) exhibits Reuss-like behavior with good agreement with measured values. The historically more widely used Kröner model produces better results for elastic constants along principal sample directions which are the preferred measurement directions of neutron diffraction. Another model that contains some measure of grain-matrix interaction is the geometric average (Matthies *et al.*, 2001). This model is not sensitive to the grain shape; it therefore lacks predictive capabilities for effects of morphological textures on elastic constants.

Elastic constants calculation – both DEC and bulk elastic constants – in the general case of multiple phases, preferred orientation, non-spherical grain shapes, and arbitrary crystallographic and specimen symmetries involves complex calculations that represent a high barrier of entry for this area of research. Recently, a software tool (IsoDEC) was made available (Gnaupel-Herold, 2023; Gnäupel-Herold, 2012, download from Gnaupel-Herold (2022)) that on the basis of the aforementioned models addresses all of the requirements for estimating elastic constants for a general polycrystalline aggregate. IsoDEC was used to calculate elastic constants for porous IN625 plasma sprayed coatings which, due to the morphological texture of the pore structure exhibited significant changes in both bulk elastic constants and DEC compared to the non-porous material. The porous coating can be seen as an extreme example of an aggregate with highly disparate constituents, with additional anisotropy due to the morphological texture.

ELASTIC CONSTANTS CALCULATION

Kröner derived two expressions for the relationships between the strain $\varepsilon_{ij}(g)$ and stress $\sigma_{ij}(g)$ of a single crystallite with the orientation g and the macroscopic stress $\bar{\sigma}_{ij}$ and strain $\bar{\varepsilon}_{ij}$

(1) $$\sigma_{ij}(g) = \left(C_{ijkl} + r_{ijkl}(g)\right)\bar{\varepsilon}_{kl}$$

(2) $$\varepsilon_{ij}(g) = \left(S_{ijkl} + t_{ijkl}(g)\right)\bar{\sigma}_{kl}$$

Here, the tensors $r(g)$ and $t(g)$ are the elastic polarization and elastic susceptibility of the grain, C and S are the bulk stiffnesses and compliances. $r(g)$ and $t(g)$ further depend on the single crystal constants $c(g)$ and the inverse Eshelby tensor w. The latter contains the grain shape.

(3) $$r_{ijkl}(g) = c_{ijkl}(g) - C_{ijkl} + c_{ijmn}(g)u_{mnkl}(g)$$

(4) $$t_{ijkl}(g) = u_{ijmn}(g)S_{mnkl}$$

(5) $$u_{ijkl}(g) = -v^{-1}_{ijmn}(g)[c_{mnkl}(g) - C_{mnkl}]$$

(6) $$v_{ijkl}(g) = c_{ijkl}(g) - C_{ijkl} + C_{ijmn}w_{mnkl}$$

Details on the calculation of the Eshelby tensor w can be found in Gavazzi's work (Gavazzi & Lagoudas, 1990). Overall force balance conditions require that in the average over all grain orientations both the polarization and the susceptibility vanish such that $\overline{r(g)} = 0$ and $\overline{t(g)} = 0$ (Kröner, 1958) which can be generalized beyond the scope of the Kröner models for multiphase aggregates as

(7) $$\sum_{\mu=1}^{N} \alpha_\mu \int t^{(\mu)}_{ijkl}(g) f^{(\mu)}(g) dg = \sum_{\mu=1}^{N} \alpha_\mu \overline{t_{ijkl}}^{(\mu)} = 0$$

(8) $$\sum_{\mu=1}^{N} \alpha_\mu \int r^{(\mu)}_{ijkl}(g) f^{(\mu)}(g) dg = \sum_{\mu=1}^{N} \alpha_\mu \overline{r_{ijkl}}^{(\mu)} = 0$$

The sums are extended over all N constituent phases with individual phase fractions α_μ and phase specific orientation distribution functions with intensities $f^{(\mu)}(g)$. Note that the inverse Eshelby tensor w_{ijkl} must be calculated for each grain shape. Both equations (7) and (8) stand for each of the 21 independent components of t and r. Equation (7) is solved for the bulk compliances S and (8) is solved for the bulk stiffnesses C. Depending on the specimen symmetry, the systems of equations can be highly over-determined (isotropic sample symmetry means two independent components S_{ijkl} vs. 21 $\sum_{\mu=1}^{N} \alpha_\mu \overline{t_{ijkl}}^{(\mu)}$). Note that individual phase components $\overline{r_{ijkl}}^{(\mu)} \neq 0$ and $\overline{t_{ijkl}}^{(\mu)} \neq 0$. Solving both equations can be computationally demanding because of their iterative nature and because of the requirement to calculate the Eshelby tensor for each grain shape at each iteration step. Lastly, (7) and (8) can be used for discrete electron backscattered diffraction data without difficulty because the integrations are numerically replaced by discrete sums anyway.

Once the bulk elastic constants are obtained from equation (7) and (8) the calculation of diffraction elastic constants (DEC) is less complicated because theory, methods and procedures are known, and computational tools are available (Gnäupel-Herold, 2012).

Lattice strain relates to macroscopic or bulk stress through

(9) $$\varepsilon(\varphi, \psi, hkl) = \frac{d - d_0}{d_0} = \frac{\partial \varepsilon(\phi, \psi, hkl)}{\partial \bar{\sigma}_{ij}} \bar{\sigma}_{ij} = F_{ij}(\varphi, \psi, hkl)\bar{\sigma}_{ij}$$

The F_{ij} are the DEC with the dimension of an inverse Young's modulus. They are calculated using the DEC equivalent of (7) and (8)

(10) $$F_{kl}(\phi, \psi, hkl) = m_i m_j \left(\hat{C} + \overline{\left(\hat{r}\left(g(\underline{m}||\underline{h}) \right) \right)} \right)^{-1}_{ijkl}$$

The inverse expression in equation (10) denotes an inverse tensor; $\hat{C}$ and $\hat{r}$ are 4th rank tensors.

(11) $$F_{kl}(\phi, \psi, hkl) = m_i m_j \left(S_{ijkl} + \overline{\left(t_{ijkl}\left(g(\underline{m}||\underline{h}) \right) \right)} \right)$$

Here, the (hkl) are the Miller indices, and (φ, ψ) are spherical polar angles describing the measurement direction **m**, with **h** being the vector of the lattice plane normal. The rotation $g(\underline{m}||\underline{h})$ are all orientations for which **m**||**h** and $\underline{m} = (cos\,\varphi\, sin\,\psi \quad sin\,\varphi\, sin\,\psi \quad cos\,\psi)$, with ψ as the angle between the scattering vector and the normal direction to the sample surface, and φ as the azimuth angle of the X-component of the scattering vector in the sample reference frame.

The significance of equations (10) and (11) is that, similar to the Voigt (uniform strain) and Reuss (uniform stress) limits, both prescribe bounds on the elastic constants, albeit with a smaller spread, and, crucially, containing elastic interaction between diffracting grains and their surrounding matrix.

In order to allow a better comparison with Young's modulus for the bulk, the diffraction elastic constants (i.e. E(hkl)) can be calculated from

(12) $$E_{hkl} = 1/F_{11}(0,90,hkl)$$

Here, the direction (0,90°) indicates the X-direction of the specimen. Bulk values for Young's modulus are obtained from

(13) $$E_{bulk} = 1/S_{11}$$

S_{11} is a component of the bulk compliance tensor obtained as a solution from equation (7). The calculations are done entirely using IsoDEC (Gnaupel-Herold, 2022).

MODEL APPLICATION

The application of the models discussed here in the full extent of their capabilities requires data on the elastic responses of the bulk and of the lattice as well as the microstructure. One such data set considered the elastic properties of IN625 plasma sprayed coating samples (Gnaeupel-Herold *et al.*, 2006). Published data include porosity (both enclosed and surface connected), lattice strains and bulk strains as well as elastic constants. The material investigated in (Gnaeupel-Herold *et al.*, 2006) can be seen as a composite of a IN625 majority phase and a pore structure (volume fraction < 5%), with the latter exhibiting both enclosed pores and surface connected pores. Another constituent phase found in the coatings was Cr_2O_3 which is present in fractions from 5 % up to 22 % by volume which changes the bulk elastic properties. For example, the aggregate value of Young's modulus E_{bulk} for a 78 % IN625 + 22 % Cr_2O_3 composite with zero porosity increases from 209.4 to 229.7 GPa at 100% IN625. However, the need for including different void orientations together with limitations of the simulation software (maximum of three constituent phases) required the exclusion of Cr_2O_3 from the multiphase calculations.

There is no data on the crystallographic texture of the IN625 coating, but there is evidence that metallic coatings deposited by air plasma spray have weak to negligible preferred orientation (Iordanova & Forcey, 1997). Therefore, the IN625 bulk phase will be assumed to have no

crystallographic texture. However, the same rapid solidification thought to be responsible for the lack of crystallographic texture also causes columnar grain shapes along the plane normal.

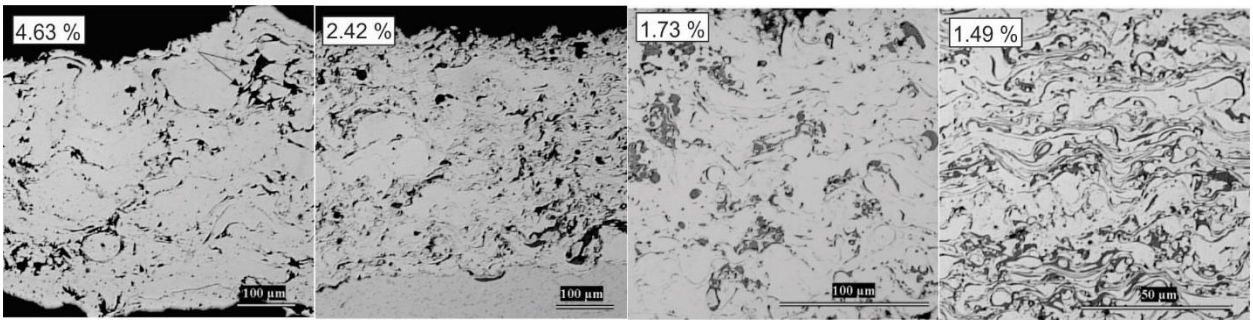

Figure 1. Micrographs of the coatings, with total porosities noted in the top left corners. Micrographs were taken with permission of the authors from (Gnaeupel-Herold *et al.*, 2006).

The void morphology is also not specified but it can be argued that the effect of void interconnectivity can be described as an increase of the void aspect ratio. The effects of void orientation, aspect ratio, and void volume fraction will be studied in more detail in the following. The microstructures of the coatings are shown in Figure 1.

The voids of a pore phase with elastic stiffnesses of zero (compliances are undefined) can have strain but not stress (see equations (1-3)). Using $c_{ijkl} = 0$ one has $r_{ijkl}(g) = -C_{ijkl}$ and equation 1) becomes $\sigma_{ij}(g) = 0$. Equation (2) is applicable to the void phase because voids can show strained; therefore equations (4) and (7) can be used to calculate the bulk elastic constants. Once the bulk elastic constants have been obtained the DEC for IN625 can be calculated from both equations (10) and (11). There are similar implications for models other than of the Kröner type in which the underlying assumptions are no longer viable. For example, the homogeneous stress condition (Reuss, Hill average) cannot lead to reasonable results since voids have no stress. Replacing zero stiffnesses with small but finite values for numerical purposes produces results that are strongly dependent on the exact values used for approximating void stiffness, thus rendering this approach unhelpful. Strain based assumptions for upper bound estimates (Voigt) as well as the geometric average (Matthies *et al.*, 2001) are valid approaches.

The single crystal elastic constants for IN625 were taken from (Wang *et al.*, 2016).

TABLE 1: Single crystal elastic constants of IN625 (Wang *et al.*, 2016) and bulk elastic constants calculated from equations (7) and (8) in the absence of porosity.

C_{11} [GPa]	C_{12} [GPa]	C_{44} [GPa]	E [GPa]	ν
243.3	156.7	117.8	209.4	0.312

IsoDEC (Gnaupel-Herold, 2022) allows for porosity in modulus calculations simply by entering zero for stiffness tensor values. However, sensible results for bulk elastic constants are only obtained with the models by Voigt, Kröner, and the geometric average. A pore population with a certain volume fraction and a given pore ellipsoid aspect ratio is considered a distinct constituent

material with elastic constants of zero. IsoDEC allows up to three constituent phases which means here IN625 as the ‘bulk’ phase and two pore phases, each with a distinct pore orientation and morphology. Pore orientations are given through the orientations of the ellipsoid axes (a=X, b=Y, c= Z).

Broader measures of the porosity in IN625 coatings were investigated (Gnaeupel-Herold et al., 2006) but data on void morphologies are not available. Different fractions of open (surface connected) and closed porosities (Table 2) can be interpreted as voids with high aspect ratio and more equi-axed, respectively.

TABLE 2: Porosity values from small angle neutron scattering (see also Gnaeupel-Herold et al., 2006). Values in brackets represent $1 \times \sigma$.

total porosity [%]	Open porosity [%]	Closed porosity [%]
1.49 (20)	1.39 (20)	0.10 (20)
1.73 (30)	0.23 (30)	1.50 (30)
2.42 (10)	2.22 (10)	0.20 (10)
4.63 (10)	4.53 (10)	0.10 (10)

The effect of spherical voids on both bulk elastic constants and DEC is shown in Figure 2, with both decreasing approximately linearly in magnitude as the porosity increases. The (311) plane was selected to allow comparison with published values. The main consequence of the grain-matrix interaction of equations (10) and (11) is that the decrease of the diffraction elastic constants with porosity is entirely caused by the decrease of the bulk elastic constants. In other words, the dependence of the bulk elastic constants on a macroscopic parameter, such as phase fraction, determines the dependence of the diffraction elastic constants for the same macroscopic parameter. Owing to the spherical shape of the voids the sample symmetry is isotropic.

Furthermore, the (311) plane represents an elastically soft direction; hence both E(311) in Figure 2 start out at lower values than E(bulk). The value from equation (10) is sometimes called the inverse Kröner value and is for isotropic materials, usually at a lower magnitude than for equation (11). E(bulk) decreases faster because the increasing porosity causes an increasing share of the strain concentrated in the voids as shape change; this observation represents a general property of a porous material. The slopes of the two DEC are slightly different as well, suggesting an intersection point at higher porosities. Directions/reflections with different (hkl) (not plotted) follow the same trend of decreasing values with increasing porosity.

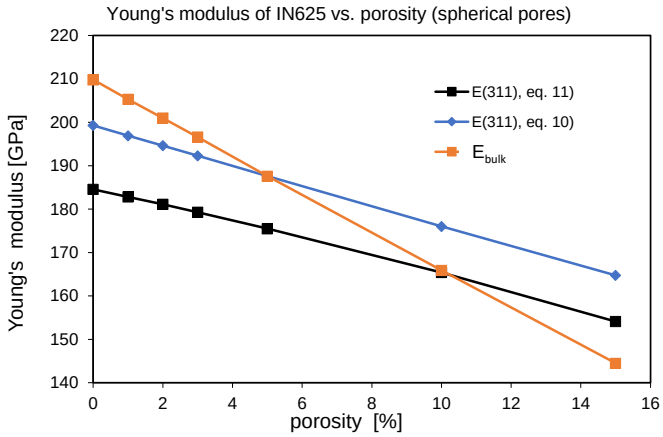

Figure 2. Bulk and DEC values for Young's modulus for spherical pores vs porosity. All values were calculated by IsoDEC. Due to isotropic sample symmetry the elastic constants do not depend on the direction. The upper/lower bound nature of equations (10) and (11) for diffraction elastic constants is apparent even when calculated for isotropic bulk elastic constants.

The decrease of the elastic constants with porosity becomes non-linear for non-spherical voids (Figure 3) which are aligned perfectly with the specimen directions X, Y, Z. The morphological texture of voids creates a highly anisotropic composite with strongly reduced values for Young's modulus E_{bulk} in the X-direction which is parallel to the short axis of the voids (oblate spheroids). The intersection of diffraction elastic constants where E(311), eq. 10 > E(311), eq. 11 happens around 1% porosity, and E_{bulk} < E(311) around 2% porosity, thus leading to the conclusion that the larger the aspect ratio the lower the porosity at which the bulk value for Young's modulus drops below the diffraction elastic constants. The upper/lower bound extremum behavior and the wide range of possible estimates for the diffraction elastic constants from equations (10) and (11) are the result of the high degree of sample anisotropy reflected in the difference between $E_{\mathrm{bulk,X}}$ and $E_{\mathrm{bulk,Y}}$.

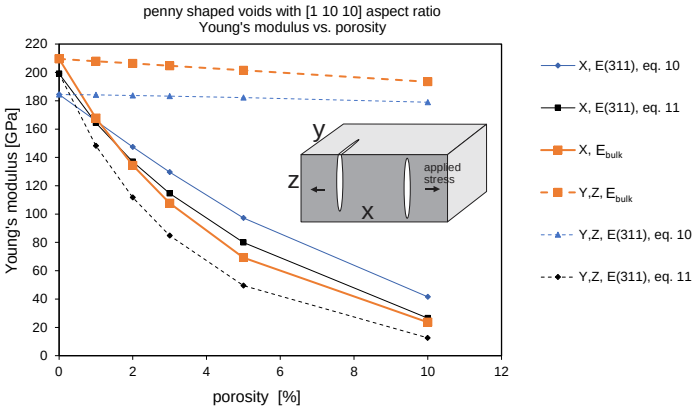

Figure 3. Calculation of Young's modulus vs porosity for penny shaped voids with [1 10 10] ellipsoid aspect ratio. The inset indicates the orientation of the voids with respect to the applied stress. The labels 'X' and 'Y,Z' denote sample directions which also coincide with the respective void ellipsoid axes.

The effect of the void aspect ratio at constant porosity (Figure 3) mirrors that of increasing porosity in Figure 3. However, bulk and diffraction elastic constants track each other more closely.

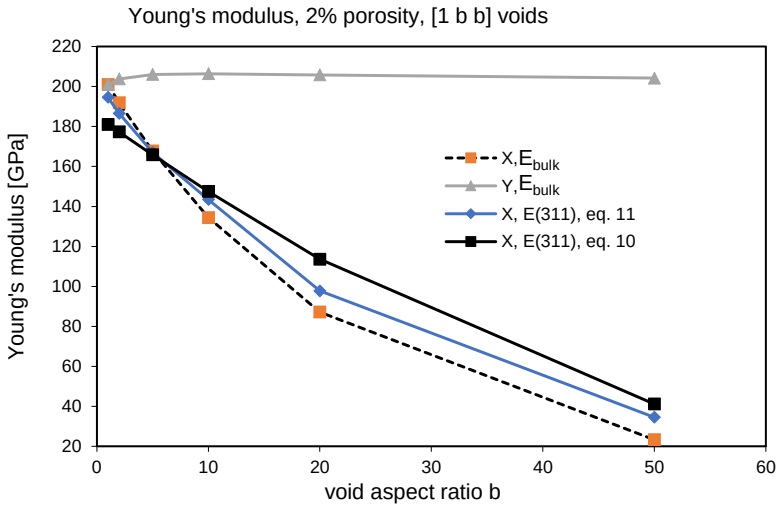

Figure 4. Calculation of Young's modulus for different void aspect ratios. The porosity is 2%. The labels 'X' and 'Y,Z' denote sample directions which also coincide with the respective void ellipsoid axes (see Figure 3 for void orientation and sample directions).

Figure 3 and figure 4 show that the two bounds calculated from equations (10) and (11) show extremum behavior which, similar to the Hill average, suggests the use of the Kröner average (equations (10) and (11)) for simplification and clarification. Also, so far simple dependencies for voids with a single orientation have been established. However, unimodal void porosity is unrealistic, and particularly the in-plane directions in plasma spray coatings are likely very similar with respect to void orientation and void aspect ratios. Figure 5 shows the effects of two void populations with the same fractions (1/2 total porosity) but different alignments along specimen axes. The voids are upright oblate spheroids, with the short dimension aligned along the coating plane X and Y.

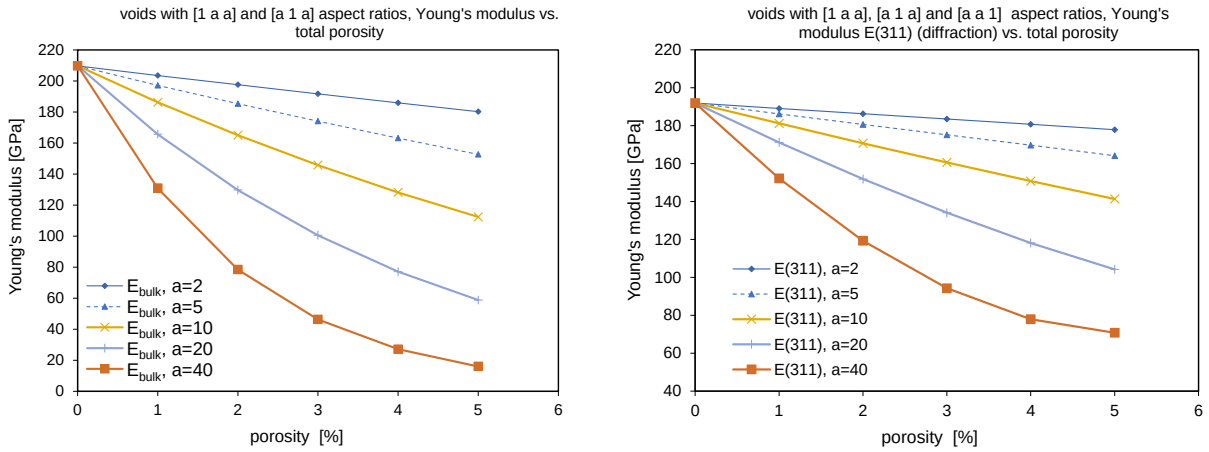

Figure 5. Calculation of the effect of porosity of two void populations with different orientation on the bulk (left) and diffraction elastic constants (right) for different void aspect ratios. The porosity fraction is evenly divided between [1 a a] and [a 1 a] voids. The diffraction modulus (right) is the arithmetic average from equations (10) and (11).

COMPARISON WITH EXPERIMENTAL DATA

Available experimental data taken from the literature (Gnaeupel-Herold *et al.*, 2006) for the porous composite discussed here include ratios of lattice strain to applied bulk strain $\varepsilon_{(311)}/\varepsilon_{bulk}$. Using

(12) $$\sigma = \varepsilon_{(311)} E(311) = \varepsilon_{\mathrm{bulk}} E_{\mathrm{bulk}}$$

this ratio can be trivially expressed as

(13) $$\frac{\varepsilon_{(311)}}{\varepsilon_{\mathrm{bulk}}} = \frac{E_{\mathrm{bulk}}}{E(311)}$$

As before, (311) refers to the Miller indices of the reflection used to measure lattice strains obtained by neutron diffraction. As shown previously, both bulk and diffraction elastic constants vary widely both with porosity and void aspect ratio parameters. Available microstructural data do not permit modulus calculation per se; however, the bulk values of Young's modulus were measured in a 4-point bending rig. The coupling between bulk values and diffraction values for Youngs' modulus from equations (10) and (11) restricts the ratio (equation 13) of elastic constants to a narrow range. As shown in Figure 5, the observed partitioning of bulk strain and lattice strain is best described as highly flattened oblate spheroid fractions with aspect ratios [1 50 50] and [50 1 50].

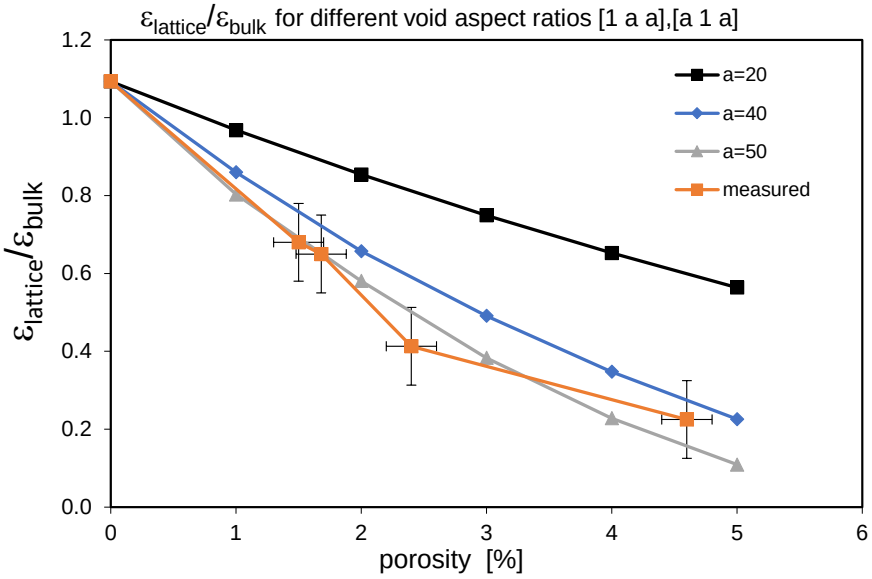

Figure 5. Comparison of ratios of lattice strain to bulk strain from (Gnaeupel-Herold *et al.*, 2006) with calculations performed in this work. The diffraction modulus values are the arithmetic average (average Kröner) of values obtained from equations (10) and (11). Total porosity is evenly divided between the two void fractions. Uncertainties represent 1×σ. Note that generally the ratio $E_{\mathrm{bulk}}/E(hkl) \neq 1$ due to elastic anisotropy in which $E(hkl)$ varies with the Miller indices.

A single aspect ratio is very unlikely but available experimental data do not allow further model refinement. Nonetheless, figure 5 shows good agreement between measured data and model prediction for [1 50 50] and [50 1 50] aspect ratios.

CONCLUSIONS

The Kröner's self-consistent upper/lower bound model was shown to be effectively used for modulus calculations of multi-phase aggregates in general and for porous composites in particular. The calculations were performed both for bulk elastic constants and, using the bulk elastic constants, for diffraction elastic constants. Utilization of the ratio of Young's modulus between bulk and diffraction values resulted in a considerable simplification and clearly showing best agreement between measurement and prediction for very high aspect ratios of oblate voids.

DISCLAIMER

Certain equipment, instruments, software, or materials are identified in this paper in order to specify the experimental procedure adequately. Such identification is not intended to imply recommendation or endorsement of any product or service by NIST, nor is it intended to imply that the materials or equipment identified are necessarily the best available for the purpose.

REFERENCES

Behnken, H. & Hauck, V. (1986). *Zeitschrift Für Met.* **77**, 620–626.

Eshelby, J. D. (1957). *Proc. R. Soc. London. Ser. A. Math. Phys. Sci.* **241**, 376–396.

Gavazzi, A. C. & Lagoudas, D. C. (1990). *Comput. Mech.* **7**, 13–19.

Gnaeupel-Herold, T., Prask, H. J., Barker, J., Biancaniello, F. S., Jiggetts, R. D. & Matejicek, J. (2006). *Mater. Sci. Eng. A.* **421**, 77–85.

Gnaupel-Herold, T. (2022). IsoDEC, version 3.03 (computer software, *Github.Com/IsoDEC/IsoDEC*.

Gnaupel-Herold, T. (2023). *J. Appl. Crystallogr., accepted for publication*

Gnäupel-Herold, T. (2012). *J. Appl. Crystallogr.* **45**, 573–574.

Gnäupel-Herold, T., Creuziger, A. A. & Iadicola, M. (2012). *J. Appl. Crystallogr.* **45**, 197–206.

Gnäupel-Herold, T., Creuziger, A. & Iadicola, M. A. (2011). *Adv. X-Ray Anal.* **55**, 128–135.

Gnäupel-Herold, T., Iadicola, M., Creuziger, A., Foecke, T. & Hu, L. (2014). *Materials Science Forum*, Vol. *768*, pp. 441–448.

Hauk, V. (1999). *Materwiss. Werksttech.* **30**, 377–384.

Hill, R. (1952). *Proc. Phys. Soc. Sect. A.* **65**, 349–354.

Iordanova, I. & Forcey, K. S. (1997). *Surf. Coatings Technol.* **91**, 174–182.

Kneer, G. (1965). *Phys. Status Solidi*. **9**, 825–838.

Kröner, E. (1958). *Zeitschrift Für Phys. A.* **151**, 504–518.

Matthies, S., Priesmeyer, H. G. & Daymond, M. R. (2001). *J. Appl. Crystallogr.* **34**, 585–601.

Reuss, A. (1929). *ZAMM - Zeitschrift Für Angew. Math. Und Mech.* **9**, 49–58.

Voigt, W. (1928). Lehrbuch der kristallphysik (mit ausschluss der kristalloptik) Leipzig, Berlin, B.G. Teuber.

Wang, Z., Stoica, A. D., Ma, D. & Beese, A. M. (2016). *Mater. Sci. Eng. A.* **674**, 406–412.